Available online at www.sciencedirect.com
ScienceDirect
Catalysis Today 129 (2007) 421–427
CATALYSIS TODAY
www.elsevier.com/locate/cattod

Photocatalytic generation of hydrogen over mesoporous CdS nanoparticle: Effect of particle size, noble metal and support

M. Sathish, R.P. Viswanath *

National Center for Catalysis Research, Department of Chemistry, Indian Institute of Technology-Madras, Chennai 600036, India

Available online 24 September 2007

Abstract

Mesoporous CdS nanoparticles with an average pore size of 54 Å and a particle size of 4–6 nm have been prepared by template free ultrasonic mediated precipitation at room temperature. The as prepared particles have been characterized by UV–vis spectroscopy, XRD, N_2 adsorption–desorption isotherms, SEM and TEM techniques. The photocatalytic hydrogen production activity for the pure, noble metal loaded and supported mesoporous CdS has been studied. The photocatalytic activity has been compared with bulk and nanosize CdS prepared in our earlier studies. Among the prepared catalysts, Pt metal loaded mesoporous CdS shows highest hydrogen production rate of 1415 μmol/h/0.1 g catalyst. In the case of supported systems, irrespective of the particle size the basic MgO support shows higher activity than alumina support.

Keywords: Mesoporous CdS nanoparticle; Hydrogen production; Effect of support; Photocatalyst; Water splitting

1. Introduction

Inorganic metal chacogenide (CdS) has received substantial attention due to their extensive application in photocatalysis [1,2]. Recent developments in nanotechnology adds further enhancement to the utility of metal chalcogenides in various disciplines. In particular, the CdS semiconductor nanoparticles have greater significance in photocatalytic hydrogen production [3–5]. The present thrust in searching a suitable material for photocatalytic hydrogen production by splitting water using sunlight as the energy source has created a considerable interest on the semiconductor nanoparticles. It has tunable band gap as a function of particle size. Also the particle size can be easily controlled by controlling the precipitation rate. As a result of tunable band gap, the electronic, optical and surface properties can be altered in the desired way. Recently it has been shown in our earlier report that the CdS nanoparticles show more photocatalytic activity for hydrogen production in presence of Na_2S and Na_2SO_3 mixture as sacrificial agent [6]. In literature, various attempts have been made to prepare CdS nanoparticles [7], nanorods [8] and nanotubes [9] for different applications. A number of methodologies like microemulsion [10], template synthesis [11,12,6], solvothermal [13,14] and γ ray irradiation [15] have been adopted to synthesize CdS nanoparticles both in aqueous and non-aqueous media. Likewise, various mesoporous materials have been synthesized via conventional approaches using surfactants as templates based on a liquid crystal template mechanism [16–18]. However, simple preparation routes for porous CdS nanoparticles have not yet been established and also with the available methods, the yield of the CdS nanoparticles is comparatively low. These methods often require a long time and multiple-step procedures. Recently, sonochemistry has been demonstrated to be an excellent method for the preparation of mesoporous materials [19–21]. It arises from acoustic activation, the formation, growth, and implosive collapse of bubbles in a liquid. The collapse of bubbles generates localized hot spots with transient temperatures around 5000 K, pressure of about 20 MPa, and heating and cooling rates greater than 109 K s^{-1} [22,23]. These conditions efficiently muddle up the cations and the anions present in the solution faster and thereby alter the rate of the precipitation reaction. In the recent past, some attempts have also been made to prepare both hexagonal and cubic CdS nanoparticles through the ultrasonic mediated precipitation at room temperature [24–26]. Unfortunately, the mesoporous CdS nanoparticles have not yet been prepared. This may be because

* Corresponding author. Tel.: +91 44 22574216; fax: +91 44 22574202.
E-mail address: rpv@iitm.ac.in (R.P. Viswanath).

0920-5861/$ – see front matter © 2007 Elsevier B.V. All rights reserved.
doi:10.1016/j.cattod.2006.12.008

of the high concentrations of the precursor solutions used in the previously reported methods. In the present study, attempt has been made to prepare mesoporous CdS nanoparticles by ultrasonic mediated precipitation using Na_2S and $Cd(NO_3)_2$ as the precursors at room temperature and the photocatalytic activity of mesoporous CdS has been studied for hydrogen production.

Generally, the photocatalytic activity has been increased by loading a suitable noble metal on the catalyst, and/or supporting the photoactive materials on a suitable support. In the former, the nature of the metal and amount of the metal loading have specific roles on the photocatalytic activity [27,28]. In the latter, the interaction between the support and active catalyst plays major role on the photocatalytic activity of the resulting catalyst. Attempts have been made to increase the photocatalytic activity of bulk CdS semiconductor by supporting it to Al_2O_3 and MgO, etc. [29,30]. It is observed that increase in the basic nature of the support increases the photocatalytic activity of bulk CdS. Efforts have been made to increase the basicity of MgO by doping with alkali metals on MgO and observed significant increment in the photocatalytic activity [30,31]. In this present study we have also attempted to increase the photocatalytic activity of prepared mesoporous CdS by loading noble metal on its surface, and supporting on Al_2O_3 and MgO support. The photocatalytic activity of mesoporous CdS has been compared with CdS nanoparticles prepared from zeolite template [6] and bulk CdS.

2. Experimental

2.1. Preparation of mesoporous CdS nanoparticle by ultrasonic method

In the typical synthesis, 250 ml of 5 mM Na_2S solution was taken in a 1000 ml glass beaker and kept in an ultrasonicator water bath. Then, 250 ml of 1 mM Cd $(NO_3)_2$ was taken in a glass syringe and slowly added into the Na_2S solution using a peristaltic pump (Miclins) at the rate of 20 ml/h. The resulting precipitate was filtered and washed with double distilled water until the solution is free form S^{2-} ions and dried in air at 120 °C for 8 h in an air oven and stored in dark coloured bottle. The CdS prepared from ultrasonic method is designated as CdS-U in subsequent discussions.

2.2. Preparation of CdS nanoparticles by zeolite as template method

The zeolite (HZSM-5) as the template, reported in our earlier publication, was employed for CdS nanoparticle preparation [6]. In a typical preparation procedure, 1 g of sodium form of zeolites was taken in a round bottom flask and 100 ml of 1 M $CdNO_3$ solution was added to it. The mixture was stirred for 24 h at room temperature. The zeolite was filtered and washed with distilled water until the filtrate is free from the Cd^{2+} ions. The sample was dried and stirred with 100 ml of 1 M Na_2S solution for 12 h resulting in the precipitation of the cadmium ions present inside the zeolite matrix. The precipitated CdS was washed with distilled water until the filtrate is free from the S^{2-} ions. Finally, the zeolite matrix was removed by treatment with 48% HF solution. The undissolved CdS was washed with hot water until the pH of the filtrate becomes neutral. The resulting precipitate was filtered and washed with double distilled water until the solution is free form S^{2-} ions. Then the powder was dried at 120 °C and calcined at 400 °C for 4 h in air. This CdS is named as CdS-Z.

2.3. Preparation of bulk CdS catalyst

The bulk CdS was prepared by conventional precipitation method by adding equimolar Na_2S and $Cd(NO_3)_2$. The resulting precipitate was filtered and washed with double distilled water until the solution is free form S^{2-} ions. Then the powder was dried at 120 °C and calcined at 400 °C for 4 h in air. The CdS particles prepared from, conventional precipitation is marked as CdS-B in subsequent discussions.

2.4. Preparation of Al_2O_3, MgO supported CdS catalyst

Different amounts of CdS, viz., 2 wt%, 5 wt%, 10 wt% and 20 wt% were supported on Al_2O_3 and MgO by dry impregnation method. For a typical synthesis, calculated amount of CdS-Z (or) CdS-U (or) CdS-B and support material (Al_2O_3 or MgO) were mixed and ground for about 15 min and calcined at 400 °C for 4 h in air.

2.5. Preparation of metal loaded CdS catalysts

Pt, Pd and Rh metal loaded CdS were prepared by wet impregnation of corresponding metal chlorides with CdS particles followed by reduction in H_2 atmosphere at 723 K. Generally, 1 wt% of noble metal was loaded over the CdS particles.

2.6. Characterization

UV–vis absorption spectra were recorded using a CARY 5E UV–vis–NIR spectrophotometer in the spectral range of 200–800 nm. The absorption spectra for the samples were recorded as a nujol paste. Powder X-ray diffraction patterns of the TiO_2 samples were recorded in a SHIMADZU XD-D1 diffractometer using Ni-filtered Cu Kα radiation (λ = 1.5418 Å). The specific surface area, pore size and pore volume of the samples were measured using a Sorptomatic (Model-1990) instrument at 77 K. Prior to the sorptometric experiment, the samples were degassed at 423 K for 12 h. Transmission electron micrographs (TEM) were recorded with a JEOL-JEM 100SX microscope, working at a 100 kV accelerating voltage. The surface morphology of the CdS particles was obtained using a JEOL-JSM-5610LV scanning electron microscope (SEM).

2.7. Photocatalytic activity

Photocatalytic hydrogen evolution experiments were performed on these materials using a quartz reactor with options

for water circulation at the outer wall of the reactor and specific outlet for gas collection. For a typical photocatalytic experiment, 0.1 g of catalyst was added to a 50 ml of aqueous solution containing 0.35 M Na_2SO_3 and 0.24 M Na_2S and placed inside the reactor. Before illumination by a UV source, the solution was de-aerated with nitrogen gas for 30 min to remove the dissolved oxygen. Then the mixture was irradiated with 400 W Hg lamp (ORIEL Corporation, USA). The evolved gas was collected over the brine water using an inverted gas burette. The gas products have been analysed using chromatograph (Nucon-Model 5765) with molecular sieve 5 Å as column and thermal conductivity detector (TCD). For the detection of hydrogen, nitrogen was used as the carrier gas and for that of oxygen/moisture, the carrier gas was hydrogen.

3. Results and discussion

X-ray diffraction patterns of as prepared CdS-U nanoparticle from ultrasonic mediated precipitation is shown in Fig. 1a (curve C). The observed peaks at "*d*" values of 1.75, 2.04 and 3.32 correspond to the (3 1 1) (2 2 0) and (1 1 1) planes with the lattice constant $a = 5.818$, show the presence of cubic crystalline phase CdS (JCPDS No.10-0454). The X-ray diffraction pattern of the as-prepared CdS-U nanoparticles has been compared with the literature reported hexagonal and cubic CdS [(JCPDS No. 06-314, JCPDS No. 1-0454, 24] in Fig. 1b and it can be clearly seen from this figure, that the diffraction angles (2θ) of the as-prepared CdS-U particles have good correspondence with the cubic CdS reported values. Peak broadening has also been observed in the as prepared CdS-U nanoparticle. The particle size has been calculated using Debye–Scherrer equation [32] and the value obtained is 4–6 nm. The as prepared, bulk and templated CdS, show no definite X-ray diffraction pattern (not shown) indicating the amorphous nature of the material. Whereas the calcined cadmium sulphide, CdS-Z and CdS-B, show presence of hexagonal crystalline future (JCPDS No.06-314), besides there is a cubic crystalline feature has also been observed in the CdS-Z sample (Fig. 1a). Due to the insignificant difference between the cubic and hexagonal reflections, the classification of cubic phase is difficult, but the peak present in the CdS-Z sample at 30° clearly indicates the presence of cubic crystalline phase. The presence of cubic crystalline phase can be attributed due to the lesser energy difference between the cubic and hexagonal phase, accordingly the cubic CdS is more easily converted to the more stable hexagonal crystalline phase during the calcination in the air. The observed sharp peak with slight beak broadening compared to bulk CdS-B sample indicates the presence of good crystalline nature of the CdS-Z sample and the peak broadening confirms the particles are in nanometer size range. It is noticed that there is good correspondence between the particle size calculated from TEM micrograph and XRD. Hence only the values obtained from TEM are given in Table 1. In the case of Al_2O_3, MgO supported CdS catalysts, the calcination at 400 °C results only the presence of hexagonal phase of CdS for all the loading, which has been clearly observed in the XRD measurement (not shown).

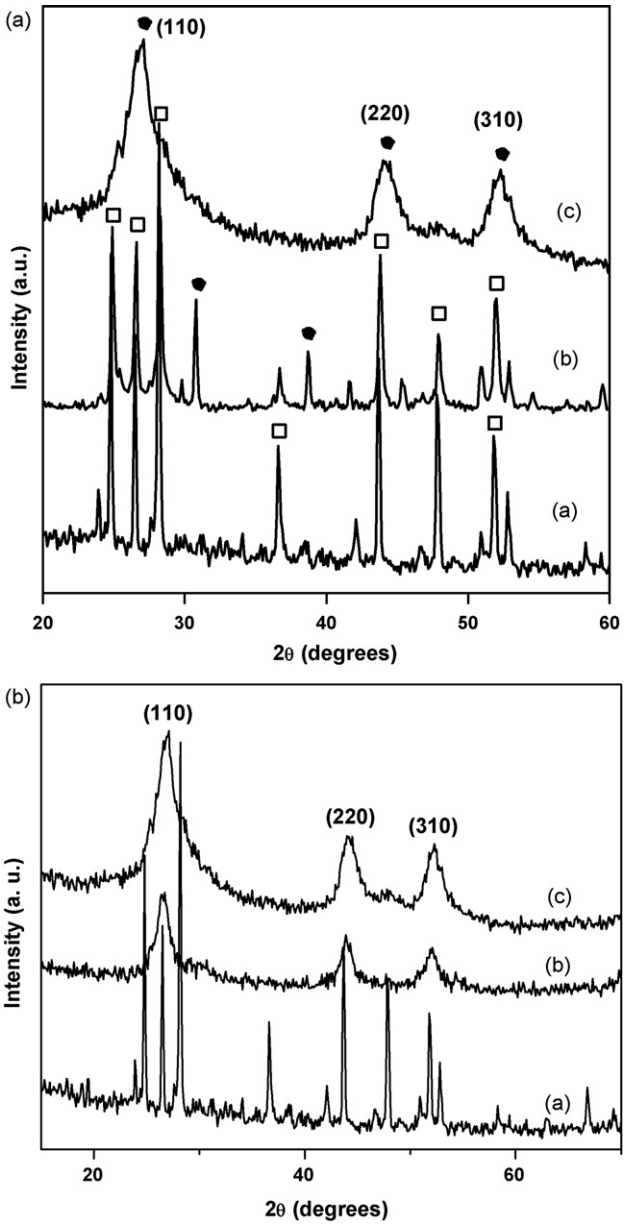

Fig. 1. (a) X-ray diffraction patterns of (a) CdS-B, (b) CdS-Z and (c) CdS-U (●, cubic; □, hexagonal). (b) X-ray diffraction patterns of (a) hexagonal CdS, (b) cubic CdS and (c) CdS-U.

UV–vis absorption spectra for CdS-Z, as prepared CdS-U and CdS-B particles are shown in Fig. 2. It can be seen that a blue shift in the onset of absorption is observed in the case of CdS-Z and CdS-U samples when compared to CdS-B, which

Table 1
Particle size, specific surface area and the rate of hydrogen evolution of CdS samples

Catalyst	Particle size (nm)	Specific surface area ($m^2\ g^{-1}$)	Rate of hydrogen evolution (μmol/h/0.1 g)
CdS-B	23	14	45
CdS-Z	6	46	68
CdS-U	5.5	94	73

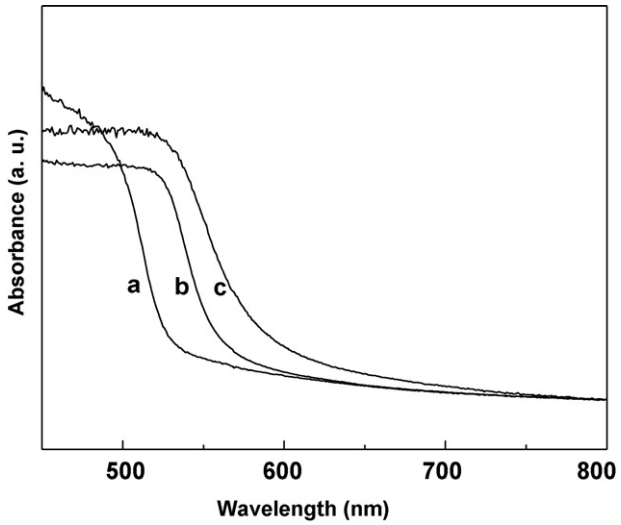

Fig. 2. UV–vis absorbance spectra of (a) CdS-Z, (b) CdS-U and (c) CdS-B.

indicates that prepared particles are lesser in size as compared to CdS-B particles. In a semiconductor, the decrease in the particle size results in the increase in the band gap between the valence band and conduction band. Consequently, the excitation of electron from valence band to conduction band requires higher energy, which results in the blue shift or light absorption in higher energy region or lower wavelength region. Though, the CdS-U particles have lesser particle size when compared to CdS-Z particles, the light absorption takes place in lower energy region or higher wavelength region compared to CdS-Z particle. This can be attributed due to the presence of cubic crystalline nature of CdS-U particle. As stated in our earlier discussion, the cubic crystalline CdS has lesser band gap than the hexagonal CdS [33]. From the above observations, it can be concluded that particle size and crystalline nature of the CdS have significant roles on the band gap of the CdS semiconductor. Besides, the UV–vis absorption spectrum of CdS-U particle shows light absorption in higher energy region when compared to hexagonal CdS-B with higher particle size, which also supports our above arguments.

The N_2 adsorption and desorption isotherms of as prepared CdS-U sample are shown in Fig. 3a. It can be seen from Fig. 3a, that the hysteresis found in this material is of type IV and can be attributed to the mesoporous nature of the as prepared CdS-U nanoparticle. The pore size distribution has been studied using B.J.H. method and is shown in Fig. 3a (inset). The specific surface area and pore volume of as prepared CdS-U sample are 95 m^2/g and 0.157 cm^3/g, respectively. It can be stated that maximum pore volume is contributed by the pores with an average size of 54 Å. Surface morphology of CdS nanoparticles has been studied by scanning electron microscopy. Fig. 3b shows that the N_2 adsorption–desorption isotherms of CdS-Z sample. It can be clearly seen from the figure that the presence of micropores on the CdS- Z samples, which can be evidenced from the observed Type I absorption isotherm with hysteresis for the CdS-Z sample. The specific surface area of the CdS-Z sample is 46 m^2/g. Where as the bulk CdS has specific surface area of ∼14 m^2/g. The observed higher surface area of the

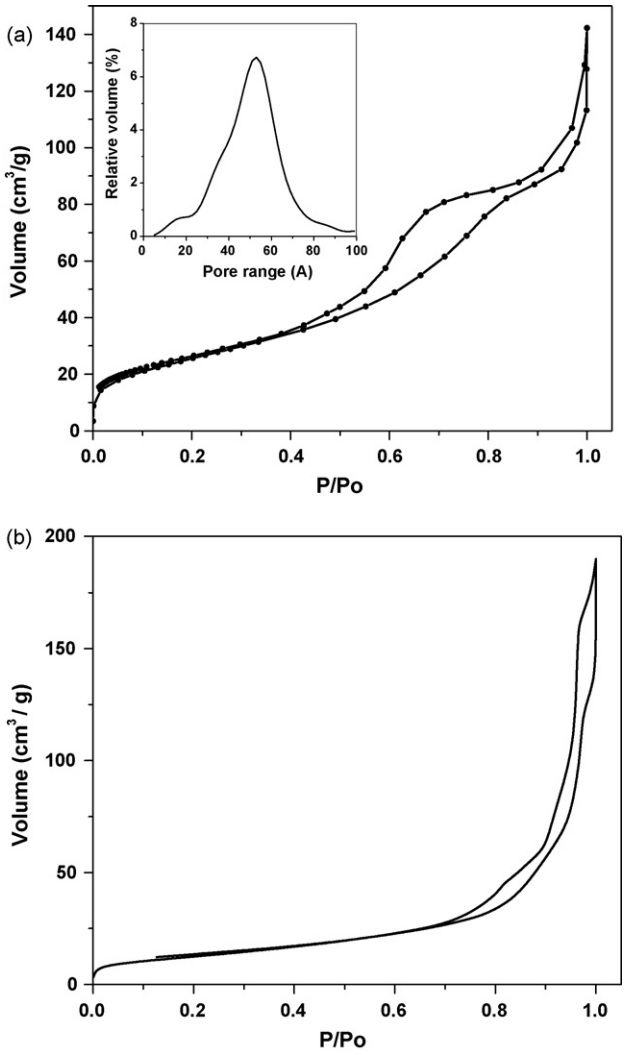

Fig. 3. N_2 adsorption desorption isotherm of (a) as prepared CdS-U particle and pore size distribution (inset) and (b) CdS-Z nanoparticle.

CdS-Z sample compared to the CdS-B is attributed to the smaller size of the particle and the presence of microporosity in the CdS-Z sample.

The transmission electron micrograph of the CdS sample is shown in Fig. 4. Particles in nanosize range are clearly observed for the CdS-U sample. The exact particle size for CdS-U has been calculated from the micrograph (Fig. 4), the fine mesoporous CdS particles in the nanosize range (4–6 nm) both in well dispersed and agglomerated forms are clearly observed for the as prepared CdS-U sample. The particle size of the bulk and CdS-Z sample has also been calculated from the micrographs (not shown) and are presented in Table 1. Surface morphology of CdS nanoparticles has been studied by scanning electron microscopy. The SEM pictures of the CdS samples are presented in Fig. 5. The growth of fine particles of CdS in a regular pattern is observed on the surface of the CdS-U and CdS-Z samples in Fig. 5a and b. In case of the bulk sample (Fig. 5c) the surface is smooth with large outgrowth of CdS particles in an irregular manner.

The amount of hydrogen gas evolved for CdS-B, CdS-Z and CdS-U are given in Table 1. From the results, it can be seen that

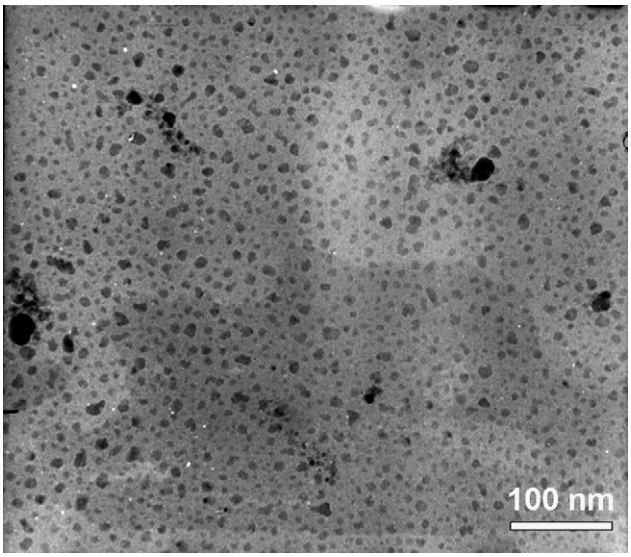

Fig. 4. TEM image of CdS-U sample.

the amount of hydrogen evolved is higher for the CdS nanoparticles in comparison with that of the bulk CdS samples. The specific surface area and the particle size are also shown in Table 1. The higher rate of hydrogen evolution can be explained by lesser particle size and higher surface area of CdS-U and CdS-Z. Although the CdS-U and CdS-Z are almost same in size, the specific surface area of the CdS-U is significantly higher than the CdS-Z particles. This may be attributed by the presence of mesopores in the CdS-U particle, which will offer higher surface area to the CdS-U particles when compared to micropore CdS-Z. Nevertheless, the photocatalytic hydrogen evolution rate for CdS-U and CdS-Z samples are comparable, this could be accounted on the basis of nature of the crystalline phase of the respective samples. The presence of hexagonal crystalline phase, which is more photoactive than the cubic crystalline phase in CdS-Z sample, enhances the photocatalytic activity of the CdS-Z sample. The particle size and nature of the crystalline phase have significant role on the photocatalytic hydrogen evolution of CdS semiconductor.

It is well known and also reported in literature, including our earlier report, that the photocatalytic activity of CdS increases substantially in presence of noble metal particles [6,27,28,30]. One weight percent metal (Pt, Pd, Rh) loaded samples were prepared by impregnation method and the hydrogen production activity has been studied. In our earlier study it is proved that the Ru loaded CdS samples shows lower hydrogen production activity than the pure CdS. The lesser activity was attributed due to the strong ruthenium-hydrogen bond, which inhibits the hydrogen evolution on the ruthenium surface. So, in our present study the Ru loading on CdS has been avoided. The hydrogen evolution rate for noble metal (Pt, Pd, Rh) loaded CdS-U nanoparticles are shown in Fig. 6. Among the noble metals studied, Pt metal loaded on CdS-U shows higher hydrogen evolution rate of 1415 μmol/h/0.1 g (31.7 ml of hydrogen/h/0.1 g). To the best of our knowledge, this may be the highest value so far reported in literature for CdS nanoparticles, and this value is much more higher than that of our earlier reported

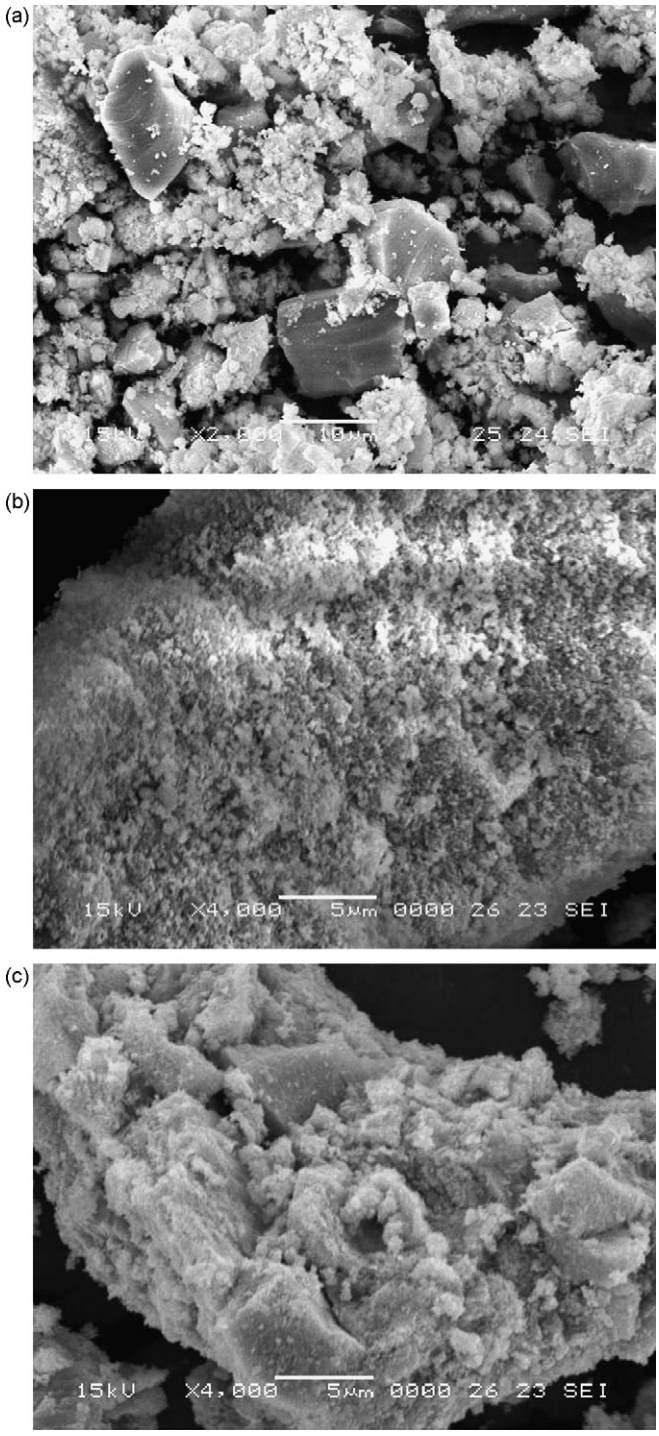

Fig. 5. SEM photographs of (a) CdS-U, (b) CdS-Z and (c) CdS-B.

value of 600 μmol/h/0.1 g for CdS nanoparticle [6]. The hydrogen evolution rate for other noble metal loaded CdS nanoparticle also show higher value and the order of the activity is Pt > Pd > Rh > Pure. Certainly, the present results support our earlier observations, and also proves that the rate of hydrogen production on a noble metal surface can be related to the metal hydrogen bond, redox potential and work function of the noble metal atom [34].

Fig. 7 shows that the photocatalytic hydrogen production activity of 1 wt% Pt loaded CdS-U, CdS-Z and CdS-B samples.

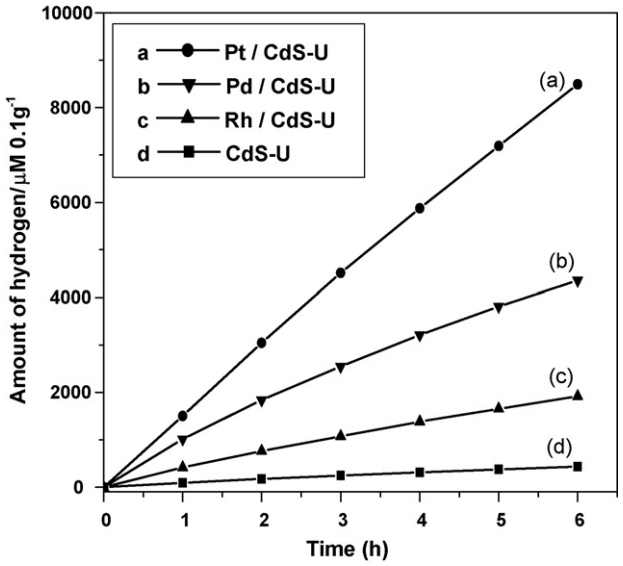

Fig. 6. Rate of hydrogen produced on CdS-U and metal loaded CdS-U samples.

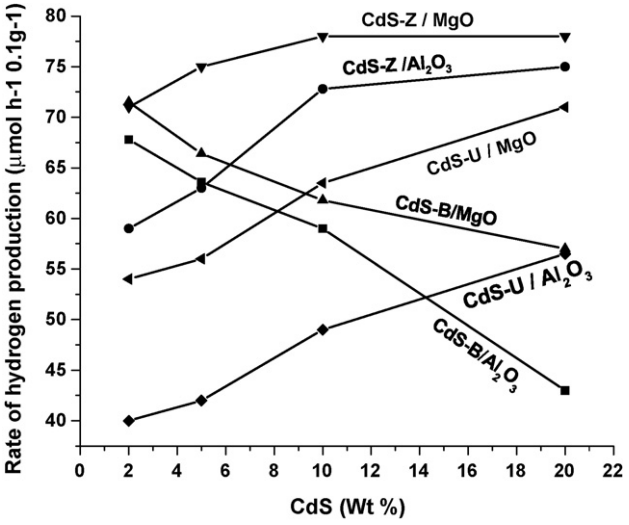

Fig. 8. Rate of hydrogen production over CdS supported on Al_2O_3 and MgO supports.

It can be clearly seen from the figure that, among the Pt loaded CdS samples, CdS-U sample shows superior activity than CdS-Z sample (∼2.4 times). In fact the CdS-Z itself ∼2.2 times more active than Pt loaded CdS-B sample. The higher activity of Pt loaded CdS-Z and CdS-U sample could be attributed to the smaller particle size. Where as, the superior activity of CdS-U is ascribed due to the good dispersion of Pt particles on the catalyst surface, the presence of mesopores in the CdS-U particles offers more surface area for the Pt particles dispersion. Also, the heat treatment during the reduction of Pt in hydrogen atmosphere at 400 °C for the Pt loading on CdS-U samples changes the crystalline nature of the CdS-U particle (not shown) i.e, phase transition will occurs from cubic to hexagonal CdS, the latter is having higher photocatalytic activity than the former.

Fig. 8 shows the rate of hydrogen production of CdS-Z, CdS-U and CdS-B supported on Al_2O_3 and MgO supports. It is well known due to the higher surface area of the support the active phase of the catalyst is well dispersed and this in turn enhances the catalytic activity. In addition to this, the nature of the support and the interaction between the support and supported materials also play an important role. For CdS-U and CdS-Z samples, increase in the rate was observed as CdS loading is increased from 2 wt% to 20 wt% on both the Al_2O_3 and MgO supports. But, in the case of CdS-B loading, when increasing CdS-B loading results a decrease in the rate of hydrogen production for both in Al_2O_3 and MgO supports. This could be ascribed due to the increase in CdS-B loading on Al_2O_3 and MgO supports results, increase the bulk behavior by this means the activity comes down towards the bulk particle, i.e. 45 μmol/h/0.1 g.

A clear increment in the hydrogen evolution rate can be seen for CdS-U and CdS-Z supported on Al_2O_3 and MgO sample when the weight % of CdS loading increases from 2% to 20%. Between the CdS-U and CdS-Z, the latter shows higher activity than the former; however the CdS-Z sample shows saturation in the hydrogen evolution rate at 20 wt% loading on both Al_2O_3 and MgO support. It is speculated that due to the complete coverage of the support surface at the higher loading of the active materials may hinder the further increment in the hydrogen production activity. Whereas in CdS-U supported samples, though the hydrogen production activity is lower than corresponding CdS-Z supported samples, there is a significant increment for each higher loading up to 20 wt% studied. The lower activity of CdS-U supported systems is believed to be due to non-availability of large surface area of mesopores CdS-U; the mesopores may be blocked by support material. This observation sustains our earlier speculation that the increase in the loading after certain extent completely covers the support surface thereby by the further enhancement in the activity has been stopped. The studies on CdS-B supported on MgO and Al_2O_3 systems show comparable hydrogen production activity at the lower loading (2 wt%), whereas the further loading of CdS-B on the both the supports shows deceases in the activity, and at 20 wt% loading, the activity is almost more or less equal

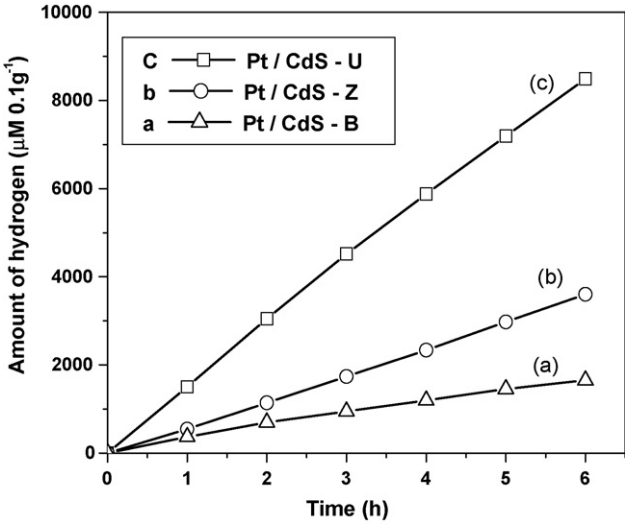

Fig. 7. Hydrogen production rate on Pt loaded (a) CdS-B, (b) CdS-Z and (c) CdS-U samples.

Table 2
Rate of hydrogen evolution (μmol/h/0.1 g) of supported CdS Samples

Catalyst	*X*		
	CdS-U	CdS-Z	CdS-B
5 wt% *X*/Al_2O_3	42	63	64
10 wt% *X*/Al_2O_3	49	73	59
5 wt% *X*/MgO	56	75	66
10 wt% *X*/MgO	64	78	62

to unsupported CdS-B. This observation strongly supports our speculation, that the activity is retained after the complete coverage of support surface; the further increase in the loading may decrease the activity of the catalyst due to the bulk behavior. Another interesting observation is, irrespective to the particle size of CdS, MgO support shows higher rate of hydrogen production rate than the Al_2O_3 support (Table 2). Higher activity for the MgO support compared to the Al_2O_3 support is due to the more basic nature of the MgO. It has also been reported in the literature, when the basic nature of the support increases, the photocatalytic hydrogen production activity increases [30]. Modification of the bascity of MgO with alkali metal doping on MgO supports results change in the hydrogen evolution rate [31].

4. Conclusions

Mesoporous CdS nanoparticles have been prepared by template free ultrasonic mediated precipitation method. This method even without calcinations enables us to prepare cubic crystalline CdS nanoparticles in the range of 4–6 nm in size. The photocatalytic hydrogen production activity of the as prepared and noble metal loaded mesoporous CdS nanoparticle was evaluated. The photocatalytic activity of the mesoporous cubic CdS was compared with CdS nanoparticle and CdS bulk particle. Among the prepared catalyst Pt loaded mesoporous CdS nanoparticle shows higher activity. The effect of support on the photocatalytic hydrogen production activity of CdS has been studied by using Al_2O_3 and MgO as supports. Between the supports, the basic MgO support shows higher activity for the hydrogen production both for bulk and nanosize CdS.

Acknowledgements

We thank Department of Science and Technology (DST), New Delhi, India, for research funding and University Grant Commission (UGC), New Delhi, India, for fellowship to one of the authors M. Sathish.

References

[1] K. Kalyanasundaram, M. Graetzel, E. Pelizzetti, Helv. Chim. Acta 65 (1982) 243.
[2] S. Kodama, A. Matsumoto, Y. Kubokawa, M. Anpo, Bull. Chem. Soc. Jpn. 59 (1986) 3765.
[3] J.R. Darwent, G. Porter, J. Chem. Soc., Chem. Commun. 4 (1981) 145.
[4] M. Matsumura, Y. Saho, H. Tsubomura, J. Phys. Chem. 87 (1983) 3807.
[5] L.F. Dong, J. Jiao, M. Coulter, L. Love, Chem. Phys. Lett. 376 (2003) 653.
[6] M. Sathish, B. Viswanathan, R.P. Viswanath, Int. J. Hydrogen Energy 31 (2006) 891.
[7] M. Pattabi, J. Uchil, Sol. Energy Mater. Sol. Cells 63 (2000) 309.
[8] Y.T. Chen, J.B. Ding, Y. Guo, L.B. Kong, H.L. Li, Mater. Chem. Phys. 77 (2002) 734.
[9] T. Peng, H. Yang, K. Dai, X. Pu, K. Hirao, Chem. Phys. Lett. 379 (2003) 432.
[10] Q. Zhang, F. Huang, Y. Li, Colloids Surf. A 257–258 (2005) 497.
[11] N.N. Parvathy, G.M. Pajonk, A. Venkateswara Rao, Nanostruct. Mater. 8 (1997) 929.
[12] H. Wellmann, J. Rathousky, M. Wark, A. Zukal, G. Schulz-Ekloff, Micropor. Mesopor. Mater. 44–45 (2001) 419.
[13] D. Xu, Z. Liu, J. Liang, Y. Qian, J. Phys. Chem. B 109 (2005) 14344.
[14] J. Yao, G. Zhao, D. Wang, G. Han, Mater. Lett. 59 (2005) 3652.
[15] C. Xu, Y. Ni, Z. Zhang, X. Ge, Q. Ye, Mater. Lett. 57 (2003) 3070.
[16] N. Perkas, O. Palchik, I. Brukental, I. Nowik, Y. Gofer, Y. Koltypin, A. Gedanken, J. Phys. Chem. B 107 (2003) 8772.
[17] C. Yu, B. Tian, D. Zhao, Curr. Opin. Solid State Mater. Sci. 7 (2003) 191.
[18] Z. Qingmin, L. Yan, H. Fuzhi, G. Zhennan, J. Mater. Sci. Lett. 20 (2001) 1233.
[19] J.G. Yu, J.C. Yu, W.K. Ho, M.K.P. Leung, B. Cheng, G.K. Zhang, X.J. Zhao, Appl. Catal. A 255 (2003) 309.
[20] J.C. Yu, J.G. Yu, W.K. Ho, Z.T. Jiang, L.Z. Zhang, Chem. Mater. 14 (2002) 3808.
[21] J. Yu, M. Zhou, B. Cheng, H. Yu, X. Zhao, J. Mol. Catal. A: Chem. 227 (2005) 75.
[22] A. Gedanken, X. Tang, Y. Wang, N. Perkas, Y. Koltypin, N. Perkas, Y. Koltypin, M.V. Landau, L. Vradman, M. Herskowitz, Chem. Eur. J. 21 (2001) 4546.
[23] K.S. Suslick, S.B. Choe, A.A. Cichowlas, M.W. Grinstaff, Nature 353 (1991) 414.
[24] G.Z. Wang, W. Chen, C.H. Liang, Y.W. wang, G.W. Meng, L.D. Zhang, Inorg. Chem. Commun. 4 (2001) 208.
[25] M. Shao, Z. Wu, F. Gao, Y. Ye, X. Wei, J. Cryst. Growth 260 (2004) 63.
[26] H. Li, Y. Zhu, S. Chen, O. Palchik, J. Xiong, Y. Koltypin, Y. Gofer, A. Gedanken, J. Solid State Chem. 172 (2003) 102.
[27] T. Sakata, T. Kawai, K. Hashimoto, Chem. Phys. Lett. 88 (1982) 50.
[28] K. Kalyanasundaram, E. Borgarello, M. Graetzel, Helv. Chim. Acta 64 (1981) 362.
[29] A.S.K. Sinha, N. Sahu, M.K. Arora, S.N. Upadhyay, Catal. Today 69 (2001) 297.
[30] M. Subrahmanyam, V.T. Supriya, P. Ram Reddy, Int. J. Hydrogen Energy 21 (1996) 99.
[31] V.T. Supriya, M. Subrahmanyam, Int. J. Hydrogen Energy 23 (1998) 741.
[32] B. Cullity, Elements of X-ray Diffraction, Addison–Wesley, Reading, MA, 1987, p. 294.
[33] O.Z. Angel, J.J.A. Gil, R.L. Morales, H. Vargas, A. Ferreira da Silva, Appl. Phys. Lett. 64 (1994) 291.
[34] K.T. Ranjit, T.K. Varadarajan, B. Viswanathan, J. Photochem. Photobiol. A 96 (1996) 181.